Developing a 3D neutron tomography method for proton exchange membrane fuel cells

Hong-Yue Tang [a], Anthony Santamaria [a], Jonathan Kurniawan [a], Jae Wan Park [a,*],
Tae-Hyun Yang [b], Young-Jun Sohn [b]

[a] Department of Mechanical and Aerospace Engineering, University of California, One Shield Ave., Davis, CA, 95616-5294, United States
[b] Korea Institute of Energy Research, 71-2, Jang-dong, Yuseong-gu, Daejeon 305-343, Republic of Korea

ARTICLE INFO

ABSTRACT

Fuel cell visualization is an ongoing challenge in the world of hydrogen-based research. Neutron tomography is a powerful tool for acquiring otherwise unattainable information about the inner workings of a proton exchange membrane fuel cell. Advanced neutron imaging methods allow for validation of both cell design and run methods. The tomography techniques discussed in this paper show how 3D visualization provides a clear view of flow channel activity for water management analysis. A brief intro to tomography is explained via its mathematical construction, outlining how 2D radiographs can be reconstructed and layered to form 3D visualizations. The low attenuation aluminum cell designs used for imaging are described focusing on how they are specifically tailored for neutron tomography. Images of the flow channel and water distributions are shown in cross-sections throughout the cell, both perpendicular and along the channel length. Finally, 3D tomography images of the cell are shown, with the bipolar aluminum plates signal subtracted revealing a 3D water distribution of both cathode and anode layers.

1. Introduction

The need for non-invasive methods to analyze a proton exchange membrane fuel cell's (PEMFC) water distribution in both *in situ* and *ex situ* conditions makes neutron radiography an excellent imaging choice [1,2]. These methods are important validation tools for both research and commercial application [3,4]. Although various diagnostic techniques are available [5–7], visualization of the inner workings of the fuel cell can offer more insight for researchers and developers. While methods such as fluorescence microscopy for *ex situ* observation of the GDL [8] can provide details as to the operation of an individual component, methods for *in situ* observation are still actively researched to observe the generation of water inside the fuel cell. Some of these techniques include using novel magnetic resonance imaging methods [9], using hydrogen–deuterium to enhance contrast in nuclear magnetic resonance imaging [10], and refined neutron radiography techniques to yield high-resolution images [11–14]. Current literature contains many examples of 2D radiography images of the flow field, however, very few clear 3D tomography standards have been set [15–17]. Researchers at the National Institute of Standards and Technology (NIST) Neutron Imaging Facility (NNIF) have

acquired the first *in situ* tomographic 3D images of an operating PEMFC demonstrating the power higher quality 3D images may afford those designing a cell's water management system [18,19].

Neutron imaging is similar but complimentary to X-ray imaging, and far superior at penetrating through materials associated with fuel cell design, allowing one to observe the membrane and channel features inside a PEMFC. A collection of 2D images can be used to reconstruct a 3D image allowing for better overall visualization. Some of the key benefits that 3D imaging has over 2D imaging are: (1) Clear discernable images of both anode and cathode water distributions. (2) Close to real time imaging of all layers. (3) Detailed water distribution within each channel. Fig. 1 shows a schematic of a PEMFC. During operation, humidified hydrogen and oxygen are combined on a proton exchange membrane to produce electricity and water. Water is needed in the membrane to allow the migration of protons through the membrane. Low humidity in the membrane will inhibit the proton migration, while high humidity or flooding will prevent oxygen from reacting on the catalyst/membrane interface. The management of this water is a major area of research currently receiving lots of attention due to its relationship to overall cell performance [1,6,20–23].

Our group has set out to produce clear 3D tomography PEMFC images and demonstrate further the benefits it has over the 2D techniques. This technique will be used to validate our research work on subzero temperature fuel cell start-up and passive flow channel design in conjunction with improving water removal by

* Corresponding author. Tel.: +1 530 752 5559; fax: +1 530 752 4158.
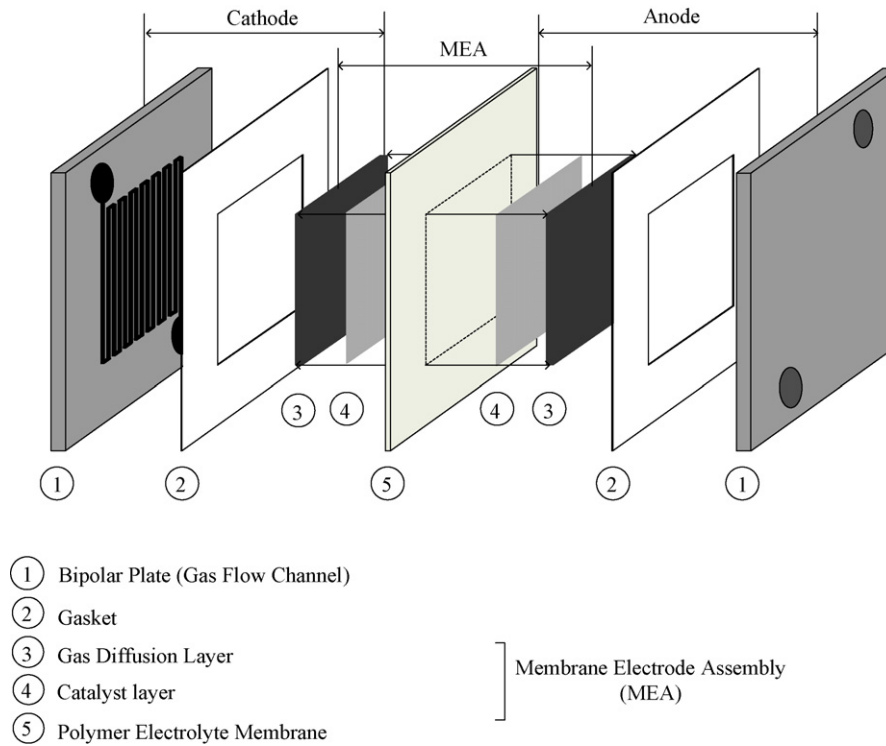E-mail address: jwpark@ucdavis.edu (J.W. Park).

Fig. 1. A simplified schematic of a proton exchange membrane fuel cell.

① Bipolar Plate (Gas Flow Channel)
② Gasket
③ Gas Diffusion Layer
④ Catalyst layer
⑤ Polymer Electrolyte Membrane

Membrane Electrode Assembly
(MEA)

means of hydrophobic/hydrophilic surfaces. This paper presents some of the imaging results of an *ex situ* PEMFC and explains the imaging process/technique used. The cells presented in this paper were designed for *in situ* testing/imaging which we hope to demonstrate in future results.

2. Background of neutron tomography

Tomography is a technique by which a series of 2D radiography image slices are reconstructed to form a 3D object [24]. The basis of radiography is that different materials attenuate a neutron beam according to their unique neutron cross section, leading to different image signatures. In the case of a PEMFC, water has a high attenuation and shows up a darker color when imaged. The beam attenuation follows the Lambert–Beer law

$$I(x, y) = I_0 e^{-\sum_i (N\sigma t)_i} \tag{1}$$

where I_0 is the initial beam intensity, I is the attenuated beam intensity, N is the atom density, σ is the material attenuation coefficient and t is the material thickness [14]. The object is scanned in incremental angles over 180° to attain all information needed to reconstruct it. Each scan creates a map of the 2D object profile as an attenuation profile parallel to the beam. The following discussion is based on the methods outlined by Treimer [24]. Eq. (1) may be written as

$$I(x, y) = I_0 e^{-\int \mu(x,y) \cdot ds} \tag{1.1}$$

where $\mu(x, y)$ is the 2D position-dependent attenuation profile to be reconstructed. The integral is taken along the path of the beam and the coordinate system used can be reassigned to express the alignment of the detector. Since we are rotating our object in place along the z-axis, the source and detector remain in the same position and it is the objects angle θ that changes. The attenuation profile is then

defined as

$$P_\theta(t) = ln\left(\frac{I_0}{I}\right) = \int \mu(x, y) \cdot ds \tag{1.2}$$

where t is now a coordinate variable based on replacing the (x, y) system with a (t, s) system via the transform $t = x \cos(\theta) + y \sin(\theta)$. The set of projections $P_\theta(t)$ is called the Radon transform of $\mu(x, y)$, see Fig. 2. Using Fourier slice theorem, the projections can be reconstructed to form the 2D images of the object. The Fourier analyses will be omitted from this paper as we are presenting only a brief overview of the tomography technique. The 2D image slices can be reassembled to form the 3D model which is the topic of Section 4. Further reading on tomography can be found in the sources listed.

3. Experimental procedure and setup

3.1. Cell design

The ASTM E748 Standard lists the neutron attenuation coefficients for various materials, these can be found in Fig. 3. In order to
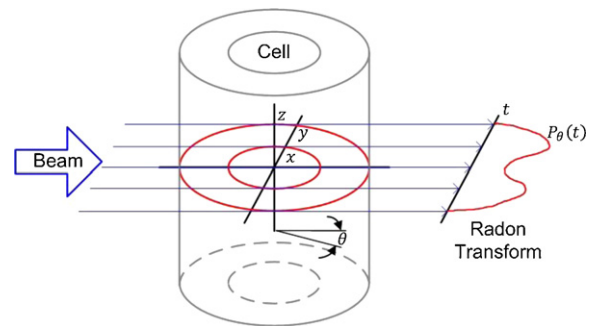

Fig. 2. The basic principle of neutron tomography. The cell is represented by a cylindrical geometry for simplicity. Each radiograph projection, $P_\theta(t)$, contains the attenuation data x, y and dz of the actual object for a $d\theta$.
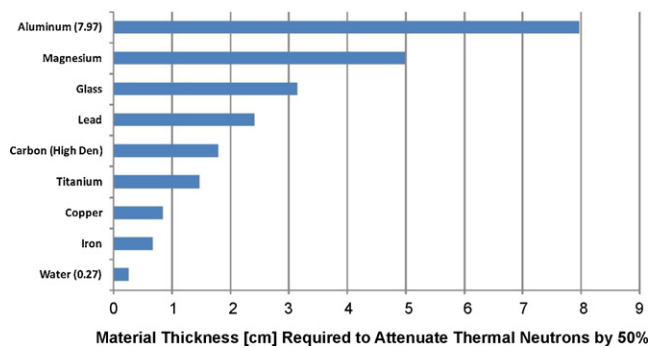
Fig. 3. Material thickness required to attenuate 50% of thermal neutrons [33].

achieve the best imaging results a fuel cell was designed specifically for tomography. Since it is desirable to reduce attenuation caused by the cell body, aluminum was chosen for the bipolar plates construction. Fig. 4 is the completed cell design as well as stainless Swagelok fittings. The gas inlets and outlets were designed so that all ports could be connected via a single surface of the cell to prevent interference during the rotation needed for tomography. In this *ex situ* example, however, reactant gas line interference would not be an issue since the cell would be pre-run and the inlets and outlets capped off to seal in the water. Other machined features and connecting hardware in the bipolar plates were designed so there would be no interference between them and the flow channels when the cell is rotated about the cells *z*-axis.

Two test cell geometries are used in the setup: cylindrical and planar. A cylindrical cell was specifically designed to give uniform attenuation in 3D tomography. In 3D tomography, the fuel cell must be rotated to obtain a series of radiography data for the 3D reconstruction. Using the round cell provides a smoother radiograph thus reducing the effort in the image post processing steps. A planar cell is designed to minimize the distance between the fuel cell and the scintillation screen in order to obtain a higher contrast image of the flow field. This is useful in studying diffusion especially during *in situ* experiments. For studying serpentine flow field channel patterns the flat cell is designed with the cathode and anode channels aligned perpendicular to each other. This makes discerning the anode and cathode sides, during *in situ* water formation, from one another possible. This is advantageous for studying membrane performance and flow channel design. Fig. 4 includes the computer rendered design images of the test cells.

Although not the focus of this paper, the run conditions of the cells prior to *ex situ* imaging were the following: inlet gas temperatures of both H_2 and Air were maintained at 80 °C. The inlet H_2 was fed at 100% relative humidity. The cell body was maintained

at 80 °C using cartridge heaters and was run at a constant voltage of .5 V until steady state operation was reached. The cell was shutdown without purging and allowed to cool before imaging.

3.2. Imaging setup

The McClellan Nuclear Radiation Center is an experimental TRIGA reactor that is rated for 2 MW steady state operation with a pulse capability of approximately 1000 MW for 20 ms [25]. The facility was designed for military component inspection and is now owned by the University of California, Davis and made available for PEMFC research. Of the four imaging bays at MNRC, two bays are equipped to perform 3D tomography. They are each setup for different neutron beam intensities for different imaging needs. Bay 3 supplies higher beam energy resulting in shorter exposure times, while Bay 4 is a lower beam energy but larger focal length to aperture ratio resulting in clearer images. Table 1 summarizes the characteristics of Bays 3 and 4.

For 3D tomography, the test cell is mounted in a Jacob chuck on a rotating table, see Fig. 5. The exposure time ranges from 30 to 180 s or more depending on the lens, neutron beam intensity, scintillation screen and camera settings. A series of radiographs are taken at each incremental angle, then are post-processed to obtain the final images. Large pieces of lithium are used to isolate unused portions of the scintillation screen to reduce noise and to protect the camera equipment from exposure. It should be noted that after the imaging process has been concluded, the cells must be left at the facility until their radioactivity levels have dropped to safe handling conditions, usually several hours to a day.

3.3. Imaging processing

Radiograph data from the tomography was reconstructed using Lawrence Livermore National Lab's Imgrec reconstruction software developed by Dan Schneberk. The raw radiographs taken from each angle were compiled into a directory and would serve as the basis for volume reconstruction [26]. To ensure clean image results, two types of calibration images were taken for calculation of attenuation coefficients and the reduction of error. One image is taken with no incident radiation, called the dark field image, and the second is taken with full incident radiation but no cell in the beam path, called the flat field image. These images are used to calibrate the raw intensity counts and calculate total attenuation through the sample in the radiographs.

As discussed earlier in the tomography section, the raw projections, $P_\theta(t)$, can be plotted as a Radon transform, displaying an attenuation radiograph with respect to cell rotation angle. This plot, also called a sinogram, allows the reconstruction of a cross section
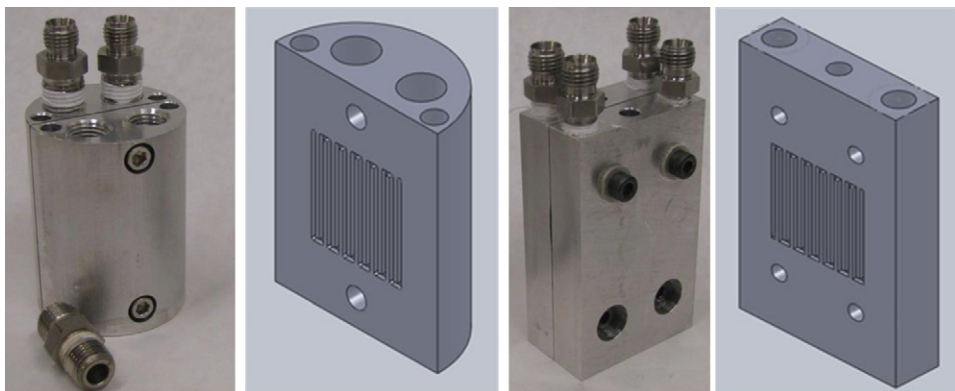

Fig. 4. Custom fuel cells made with aluminum bipolar plates. These test cells are designed to minimize the neutron attenuation effects in order to give the clearest image of the flow channel and MEA.

Table 1
Summary of the imaging capabilities of Bay 3 and Bay 4 at MNRC.

|	Bay 3	Bay 4
Angle from the horizon	$-30°$	$-20°$
Neutron thermal flux	$\sim 1 \times 10^7 \, \mathrm{n \, cm^{-2} \, s^{-1}}$	$\sim 7 \times 10^6 \, \mathrm{n \, cm^{-2} \, s^{-1}}$
Scintillation screen resolution	$100 \, \mu\mathrm{m}$	$\sim 200 \, \mu\mathrm{m}$
Camera	Apagee Alta	Photometrics/Roper Scientific Quantix
Camera operating temperature	-25 to $-20°C$ Thermoelectric cooling	-32 to $-29°C$ Thermoelectric cooling liquid N_2 cooling capable
Lens	Nikon F-mount 105 mm f2.8D	Nikon F-mount 50 mm f1.2
Rotating table resolution	$0.5°$ per step	$0.5°$ per step
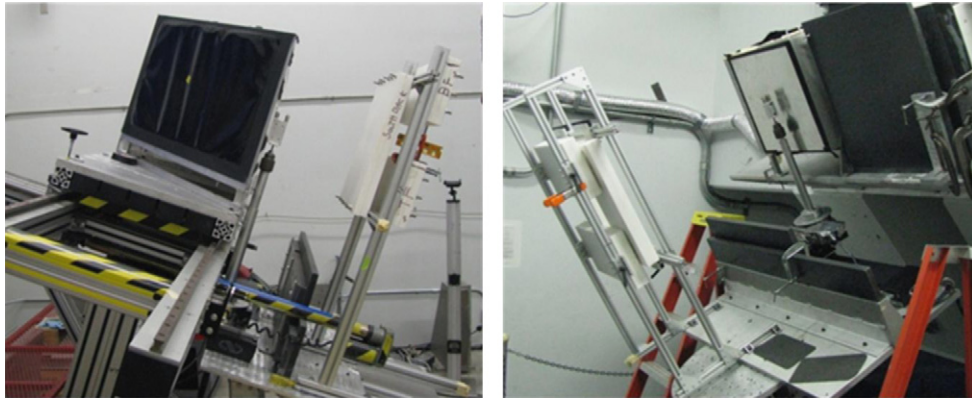
Fig. 5. The imaging fixtures in Bay 3 and 4 at MRNC. Lead and lithium shielding blocks are used to protect the camera and other electronics from high energy neutrons during imaging.

along the z direction of the sample. The dimensions of the sinogram plot are: the radiograph projection per rotation angle θ plotted against the distance x across the sample. Sinograms may contain ring artifact noise, a result of pixel response fluctuation, which can be seen as vertical stripping in the sinogram. This is corrected using both filtering and normalization processes which enhance image quality and improve accuracy. An inverse Radon transform is then applied to each sinogram to recover the actual cross sectional slice [27]. Fig. 6 shows these process steps transforming raw radiograph projections to 2D slices, along with further explanation. The collection of the reconstructed cross section slices, called the voxel data, was then loaded into post processing software to construct the 3D model.

4. Results and discussion

The 3D model created in this work allows for a clear visualization of the fuel cell interior. The model can be used to reconstruct cross sectional views of any arbitrary plane. The benefits outlined in the introduction are elaborated upon with some example images. Fig. 7 presents a set of reconstructed planar images from the MEA, anode and cathode flow channels of the planar cell. The lighter gray regions indicate high levels of neutron attenuation. Each pixel in the figure corresponds to approximately $110 \, \mu\mathrm{m}$ of real length. The anode and cathode images are obtained by overlaying 10 2D cross-sectional images in the direction normal to the plane spanning the entire depth of the flow channel. The planar image of the
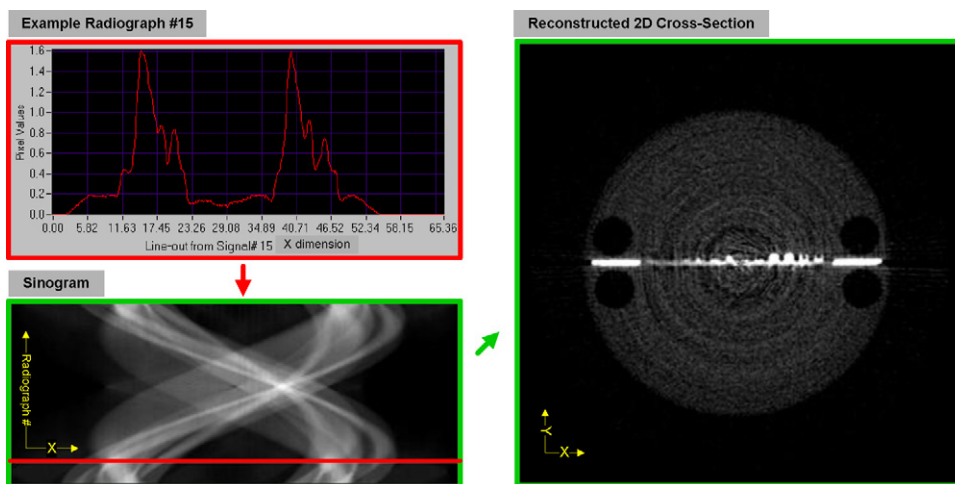

Fig. 6. After obtaining the radiographs, a series of sinograms are used to reconstruct the cross-sectional views of the object. First, the radiograph projections are plotted as a function of the object's imaging angle. The red line demonstrates a single radiograph at an angle θ, within the sinogram, hundreds may be used to construct a sinogram. All the radiographs of a single sinogram correspond to the same dz of the actual object. Finally, an inverse radon transform is then applied to each sinogram in order to reconstruct the cross-sectional slices needed for the 3D image, ie, denoted by the green borders. (For interpretation of the references to color in this figure legend, the reader is referred to the web version of the article.)
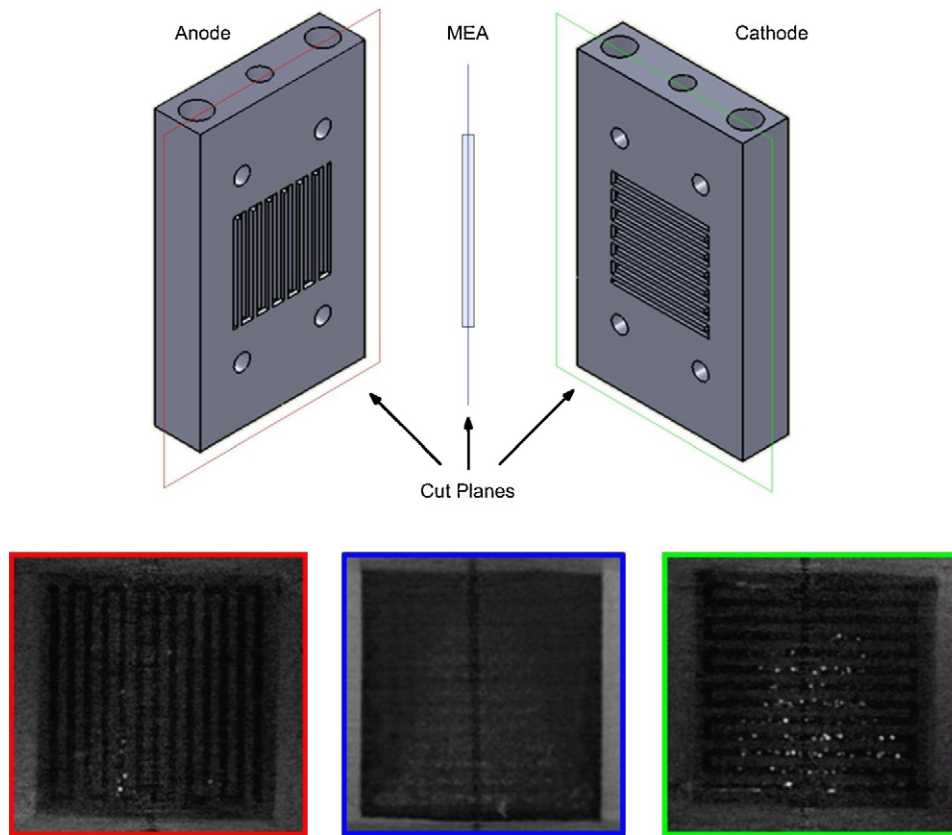
Fig. 7. Results of the 3D reconstruction of a flat fuel cell with crisscross serpentine. Individual layers can be extracted from the model to display water distribution in both the cathode and anode flow channels.

MEA includes approximately 20 μm above the surface of catalyst layer on both sides since the thickness of MEA is around 70 μm. The image contains the interfacial gap between the catalyst layer and the GDL where the liquid water formed by reaction may have accu-

mulated due to the GDL's hydrophobicity. The water distribution matches the pattern of the serpentine flow channel in Fig. 7, possibly a result of water rejection from the GDL during the time the cell was idle between operation and imaging. Although not shown,
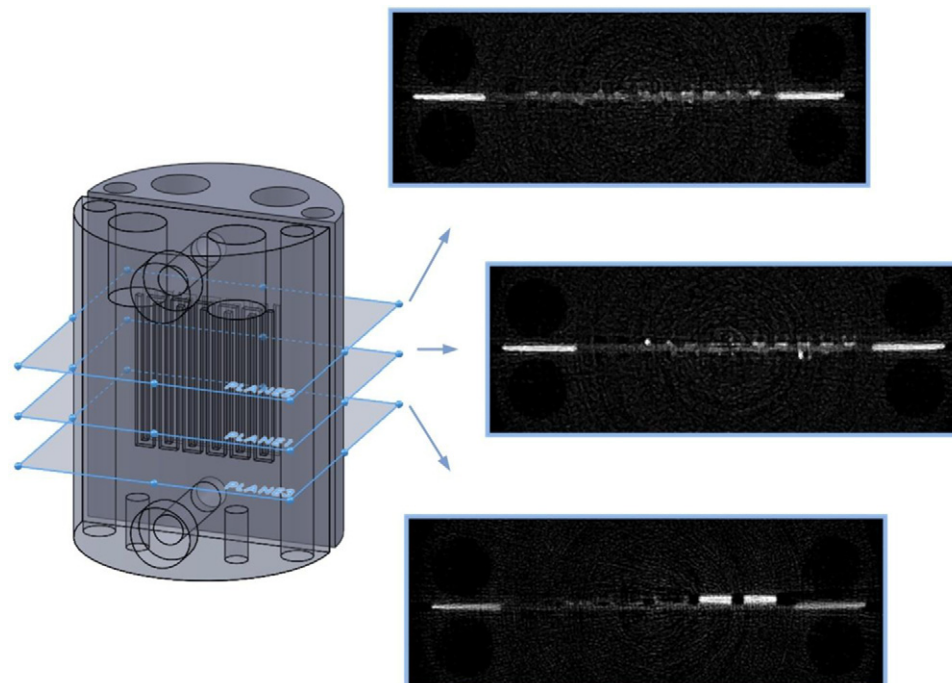
Fig. 8. Results of the 3D reconstruction of a round fuel cell with serpentine. The gasket and the water inside the flow channels give a much higher attenuation than the aluminum bipolar plates, resulting in higher contrast in the image.
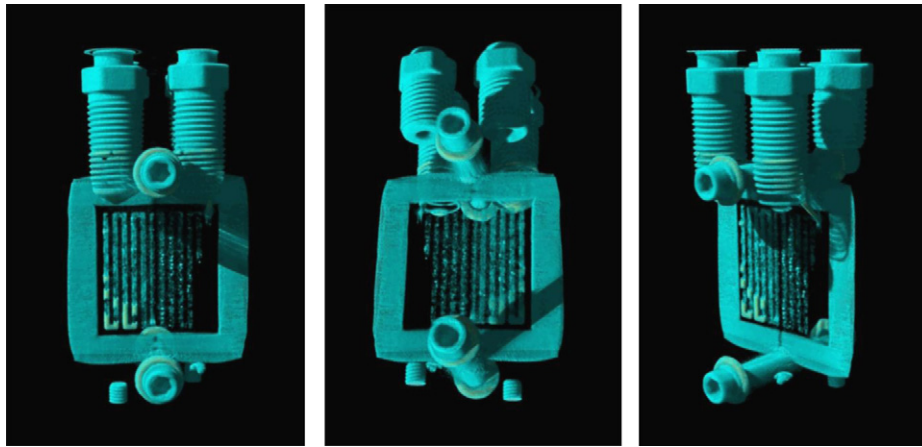
Fig. 9. Screen capture of the 3D animation rendered with the reconstructed voxel data set. The internal structure can be analyzed by freely rotating the model. Water blockages inside the flow channel can be immediately identified.

almost no trace of water was found in the GDL. The water found within flow channel area is distributed randomly in droplet form of various sizes. This is most likely water that has migrated out of the GDL via capillary action and a static pressure gradient as a result of the cell being purged before shutdown. The cathode flow channels contain more liquid water due to the fact that the oxygen reduction and water formation occurs on the cathode side while water must be transported to the anode flow channels primarily through the membrane by back diffusion from the cathode.

In Fig. 8, the images are reconstructed in a plane normal to the axis of the cylindrical cell to visualize simultaneously the water distribution in both the anode and cathode areas perpendicular to gas flow. In this case, the cell was not purged after operation and to maintain the water generated the inlets and outlets were sealed. A considerable amount of liquid water is found downstream in the cathode flow channel and has accumulated on the lower corner of the flow field possibly due to gravity. Liquid water has been produced by both reaction and condensation due to the high gas inlet humidity and significant temperature drop from its initial temperature ($80\,^\circ$C). It should be noted that the water distribution in these cell components will provide significant merit in investigating the water transport phenomenon through the membrane via back diffusion and electro-osmotic drag.

Additional full 3D model rendering was performed using the commercially available software, VG Studio, which allows for higher refined image reconstruction including volume and structural analysis, as well as animation rendering. By adjusting the visible range of the attenuation graph and histogram, the aluminum bipolar plates can be excluded from the resultant image, exposing the internal structure of the fuel cell. Fig. 9 presents several screen shots from an animation of the round cell being rotated in all directions. The rendered 3D images provide a clear view of water distribution as well as some highly attenuating cell fixtures including silicon gaskets and stainless steel fittings. More liquid water is shown downstream of the serpentine flow channel possibly due to the reactant gas flow and condensation caused by the increasing partial pressure of water vapor, i.e. reactant depletion.

Using the color and opacity manipulator, materials with similar attenuation levels can be colored or removed in the reconstructed object isolating important features. The level of attenuation in the flow channels, GDL and MEA of the cylindrical cell are colorized according to the color band shown in Fig. 10. The choice of color can also enhance the contrasts of various materials and features inside. In Fig. 11, far more liquid water is found on the cathode side and parts of the downstream channel are flooded as indicated previously. Upon inspection of the cathode GDL, the water distri-

bution is found to clearly match the flow channel pattern, i.e. more water is distributed along the flow field area while far less water is present within the GDL at regions it is in contact with the bipolar plates. This effect is known as cross leakage flow [17,22]. The image of the membrane shows a similar water distribution pattern to the cathode GDL image, this is due to water existing at the interface between the MEA and GDL most prevalently along the flow field area. Fig. 11 also shows two green highlighted boxes containing areas where water in the GDL appears to have been rejected by the hydrophobicity of the GDL into the flow channel, flooding it. Water droplets are trapped inside the GDL layer if insufficient amounts of water are present to enable capillary action to draw the water out into the flow channel. This may be attributed to the fact that capillary forces are more effective when accumulated water droplets have reached a critical size allowing them to transport out of, or permeate through, the GDL into the flow channel which has a lower hydrophobicity. When the water is in a smaller discrete droplet from, as in the case of the anode GDL, the distribution appears much more homogeneous compared to the cathode GDL. This is because there is not enough water present to interface into larger droplets, leaving the individual droplets isolated within the GDL. The differences in water distribution in the GDL may also be affected by the degree of GDL compression. Since the compression of the GDL changes the porosity and creates microfiber breakages [28], the effective hydrophobicity may be changed [29,30], thus altering the transport properties within the GDL. Moreover, the variations of permeability in the GDL due to compression will influence the reactant gas diffusivity and reaction rate [31,32], creating temperature variations thus further changing the reaction dynamics and overall water distribution.
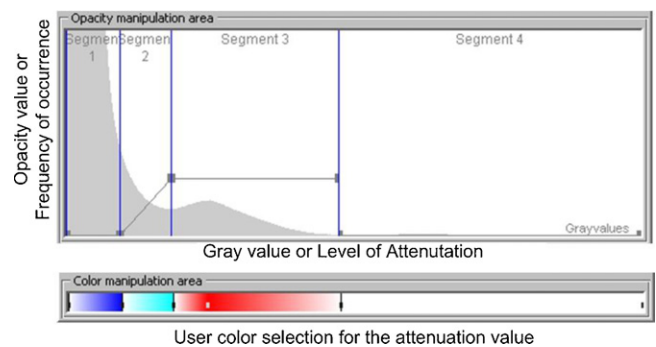
Fig. 10. User defined color manipulation and opacity settings used to classify the attenuation data.
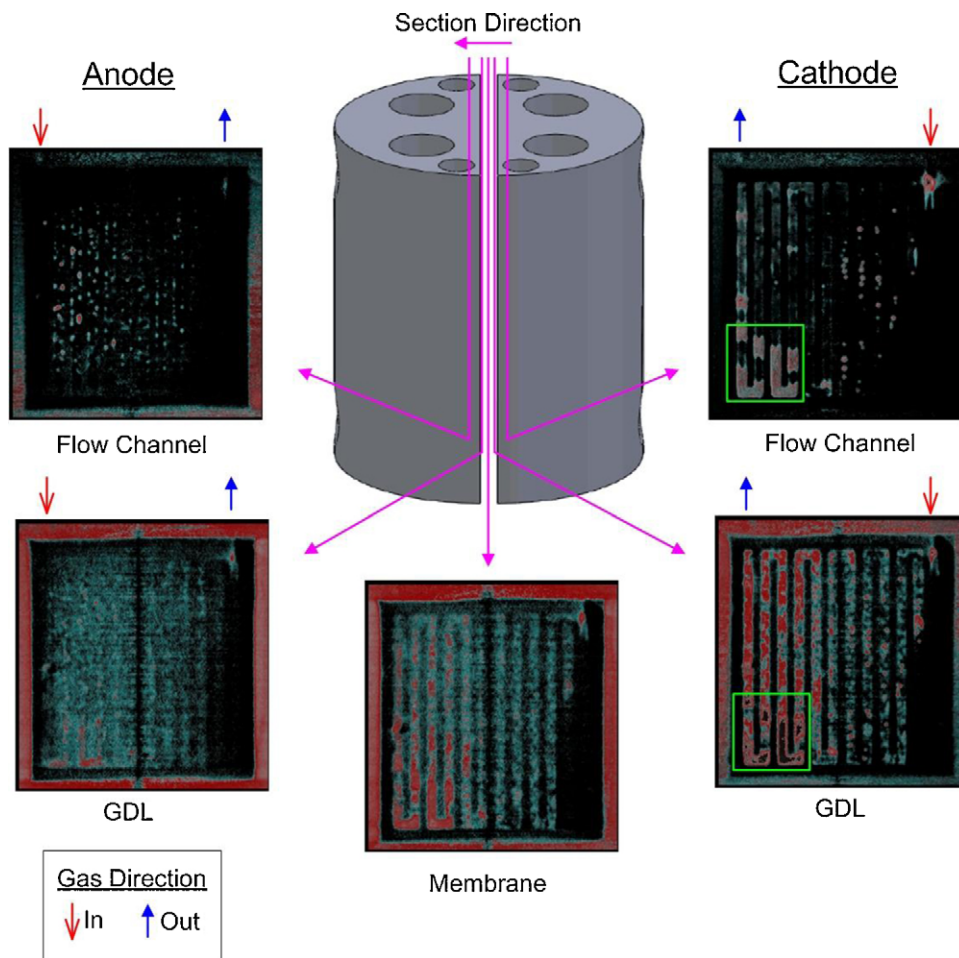
Fig. 11. Enhanced 2D image of the flow channel. The coloration can be used to help visualize the concentration of water accumulated in the MEA and flow channel. Green boxes indicate areas of discussed GDL water rejection. (For interpretation of the references to color in this figure legend, the reader is referred to the web version of the article.)

5. Summary and future work

An effective 3D tomography method has been developed to allow visualization of the internal structure of PEMFCs. This study focused on an *ex situ* cell condition, and demonstrated the improved quality such tomography techniques have over current neutron imaging standards. The images presented in this paper utilize tomography's capability to acquire all the data necessary to reconstruct an entire cell. 3D tomography makes accessible any cross-sectional view desired, providing fuel cell designers the means to test and validate different cell designs with clear comprehensive visual data. Otherwise unattainable information regarding the water distribution within the porous GDL region and the interfaces between the bipolar plates and MEA can be easily shown. Our results demonstrate several methods useful toward gaining a complete understanding of water management in a PEMFCs most critical regions.

This paper focused upon imaging techniques and quality, now that our process has been validated, our future research will aim to characterize water management and fuel cell performance. Images can be used to determine the amount of water present within the cell via calibrating the radiograph attenuation signal for a dry versus a wet flow channel region of varying thickness. This will make the accurate quantification of water creation and distribution possible in both the anode and cathode layers. These methods can also be adopted to testing fuel cells under any type of environmental and or load conditions. Used in conjunction with quantitative data,

tomography provides a powerful tool to verify simulation work with experimental results. The next level of work will be incorporating *in situ* PEFMC conditions with the imaging techniques that have been discussed. This will further enable fuel cell designers with real time visualizations of cell water management and overall performance. An environmental chamber is being designed within the MNRC to simulate various conditions PEMFCs may encounter especially in automotive use.

Acknowledgements

References

[1] H. Li, Y. Tang, Z. Wang, Z. Shi, S. Wu, D. Song, J. Zhang, K. Fatih, J. Zhang, H. Wang, Z. Liu, R. Abouatallah, A. Mazza, Journal of Power Sources 178 (2008) 103–117.
[2] A. Bazylak, International Journal of Hydrogen Energy 34 (2009) 3845–3857.
[3] J. Stumper, C. Stone, Journal of Power Sources 176 (2008) 468–476.
[4] D. Kramer, E. Lehmann, G. Frei, P. Vontobel, A. Wokaun, G.G. Scherer, Nuclear Instruments and Methods in Physics Research Section A: Accelerators, Spectrometers, Detectors and Associated Equipment 542 (2005) 52–60.
[5] J. Chen, B. Zhou, Journal of Power Sources 177 (2008) 83–95.
[6] J. Stumper, M. Löhr, S. Hamada, Journal of Power Sources 143 (2005) 150–157.

[7] N. Fouquet, C. Doulet, C. Nouillant, G. Dauphin-Tanguy, B. Ould-Bouamama, Journal of Power Sources 159 (2006) 905–913.

[8] S. Litster, D. Sinton, N. Djilali, Journal of Power Sources 154 (2006) 95–105.

[9] Z. Zhang, A.E. Marble, B. MacMillan, K. Promislow, J. Martin, H. Wang, B.J. Balcom, Journal of Magnetic Resonance 194 (2008) 245–253.

[10] K.W. Feindel, S.H. Bergens, R.E. Wasylishen, Journal of Power Sources 173 (2007) 86–95.

[11] H. Iwase, S. Koizumi, H. Iikura, M. Matsubayashi, D. Yamaguchi, Y. Maekawa, T. Hashimoto, Nuclear Instruments and Methods in Physics Research Section A: Accelerators, Spectrometers, Detectors and Associated Equipment 605 (2009) 95–98.

[12] T.A. Trabold, J.P. Owejan, D.L. Jacobson, M. Arif, P.R. Huffman, International Journal of Heat and Mass Transfer 49 (2006) 4712–4720.

[13] T. Kim, C. Sim, M. Kim, Applied Radiation and Isotopes 66 (2008) 593–605.

[14] R. Satija, D.L. Jacobson, M. Arif, S.A. Werner, Journal of Power Sources 129 (2004) 238–245.

[15] E.H. Lehmann, P. Boillat, G. Scherrer, G. Frei, Nuclear Instruments and Methods in Physics Research Section A: Accelerators, Spectrometers, Detectors and Associated Equipment 605 (2009) 123–126.

[16] M. Arif, D.S. Hussey, D.L. Jacobson, Neutron Imaging for the Hydrogen Economy, in: I.S. Anderson, R.L. McGreevy, H.Z. Bilheux (Eds.), Neutron Imaging and Applications, Springer US, New York, 2009, pp. 191–207.

[17] J. Park, X. Li, D. Tran, T. Abdel-Baset, D.S. Hussey, D.L. Jacobson, M. Arif, International Journal of Hydrogen Energy 33 (2008) 3373–3384.

[18] "NIST imaging instrument peers inside fuel cells," Fuel Cells Bulletin, vol. 2006, pp. 8-8, 2006.

[19] NIST, Neutron Tomography of Proton Exchange Membrane Fuel Cell at NIST, 2007.

[20] S. Kim, M.M. Mench, Journal of Membrane Science 328 (2009) 113–120.

[21] F.-B. Weng, A. Su, C.-Y. Hsu, C.-Y. Lee, Journal of Power Sources 157 (2006) 674–680.

[22] K. Jiao, J. Park, and X. Li, "Experimental investigations on liquid water removal from the gas diffusion layer by reactant flow in a PEM fuel cell," Applied Energy, 2009.

[23] Q. Yan, H. Toghiani, J. Wu, Journal of Power Sources 158 (2006) 316–325.

[24] W. Treimer, in: I.S. Anderson, R.L. McGreevy, H.Z. Bilheux (Eds.), Neutron Tomography in Neutron Imaging and Applications, Springer US, New York, 2009, pp. 81–108.

[25] MNRC, "McClellan Nuclear Research Center," 2003. http://mnrc.ucdavis.edu/imaging.html.

[26] N. Huerta, Imgrec User's Manual, 2006.

[27] F. Natterer, F. Wübbeling, Mathematical Methods in Image Reconstruction, 1st ed., 2001.

[28] Z.Y. Su, C.T. Liu, H.P. Chang, C.H. Li, K.J. Huang, P.C. Sui, Journal of Power Sources 183 (2008) 182–192.

[29] J.H. Nam, M. Kaviany, International Journal of Heat and Mass Transfer 46 (2003) 4595–4611.

[30] J.H. Nam, K.-J. Lee, G.-S. Hwang, C.-J. Kim, M. Kaviany, International Journal of Heat and Mass Transfer 52 (2009) 2779–2791.

[31] D.H. Ahmed, H.J. Sung, J. Bae, International Journal of Hydrogen Energy 33 (2008) 3786–3800.

[32] A. Bazylak, D. Sinton, Z.S. Liu, N. Djilali, Journal of Power Sources 163 (2007) 784–792.

[33] A E748-02, Standard Practices for Thermal Neutron Radiography of Materials, ASTM International, West Conshohocken, PA, 2008.